RSC Advances

ROYAL SOCIETY OF CHEMISTRY

www.rsc.org/advances

Colourimetric Assay for β-estradiol Based on Peroxidase-like Activity of Fe_3O_4@mSiO$_2$@HP-β-CD Nanoparticles

Shoulian Wei [a], Jianwen Li [b], Yong Liu [a,*]

[a] Faculty of Chemistry and Chemical Engineering, Zhaoqing University, Zhaoqing, 526061, China

[b] Department of Chinese Medicine and Biology, Guangdong Food and Drug Vocational College, Guangzhou 510520, China

Abstract: Magnetic mesoporous nanoparticles Fe_3O_4@mSiO$_2$ were prepared through co-precipitation and tetraethoxysilane hydrolysis at 60 °C and pH 10 with hexadecyl trimethyl ammonium bromide as the template. Hydroxypropyl β-cyclodextrn was modified onto Fe_3O_4@mSiO$_2$ under sodium citrate and N_2 protection via an ultrasound process to increase the catalytic efficiency. The prepared nanoparticles were characterized by Fourier transform infrared spectrometry, X-ray diffraction, scanning electron microscopy and peroxidase-like activity assay. Results showed that the prepared nanoparticles have magnetic property, peroxidase-like activity and loose spherical clusters structure. Compared with Fe_3O_4@mSiO$_2$ nanoparticles, Fe_3O_4@mSiO$_2$@ HP-β- CD nanoparticles exhibit higher catalytic ability toward both H_2O_2 and 3,3′,5,5′-tetramethylbenzi- dine. Fe_3O_4@mSiO$_2$@HP-β-CD nanoparticles can catalyse β-estradiol (β-E_2) oxidation in the presence of H_2O_2 and be used as a colourimetric sensor for indirect detection of β-E_2. Good linear relationship was obtained from 0.8 μM to 16 μM. The limit of detection of the proposed method was 0.2 μM. The visual method was successfully used in the analysis of β-E_2 in commercial tablets and animal feeds, with recovery ranging from for 92.6% to 110%.

Keywords: Fe_3O_4@mSiO$_2$@HP-β-CD; Colourimetric detection; Peroxidase-like activity; β-estradiol

1. Introduction

β-Estradiol (β-E_2) is naturally present in females and it is responsible for the growth of breast and reproductive epithelia, maturation of long bones, regulation of lipoprotein synthesis, prevention of urogenital atrophy, maintenance of cognitive function and development of

* Corresponding author at: Faculty of Chemistry and Chemical Engineering, Zhaoqing University, Zhaoqing, 526061, P.R. China
E-mail: lygdut@163.com (Yong Liu).

secondary sexual characteristics [1]. β-E_2 is mainly used as menopausal hormone and in replacement therapy of female hypogonadism or primary ovarian failure. In addition, European and Chinese legislations have banned the use of β-E_2 for growth promoters in livestock since 1988 and 2002, respectively. However, epidemiological data show that β-E_2 is still being used illegally [2]. β-E_2 is involved in endocrine disruption, thereby causing adverse health effects. β-E_2 can induce an estrogenic response and interfere with the normal endocrine function, causing the development of hormone-related carcinomas in humans and wildlife even at low concentrations [3]. Thus, β-E_2 routine analysis is necessary for quality control and drug testing-laboratories in commercial tablets and animal feeds. Several methods have been employed to determine β-E_2 in tablets and feeds, such as high-performance liquid chromatography [4], UV spectrophotometry [5], voltammetry [6], Fluorescence resonance energy transfer [7] and enzyme-linked immunosorbent assay [8]. However, the application of these methods encounters several drawbacks, such as high cost, low sensitivity, and non-visual. Thus, an economical, sensitive, simple and visual method is urgently needed to daily monitor β-E_2 in commercial tablets and feeds.

Colourimetric sensors have attracted much interest because they provide naked-eye readout signals without using expensive instrumentation, and they are suitable for on-site and real-time determination. Colourimetric sensors based on peroxidase-like activity are an important colourimetric tool to transform detection events into colour changes. Some nanomaterial, such as magnetite nanoparticles [9-10], gold nanoparticles [11], and carbon-based nanomaterials [12-13] have been reported and reviews [14] to exhibit peroxidase-like activity. Since Fe_3O_4 magnetic nanoparticles (MNPs) were found to possess the peroxidase-like property in 2007, a significant amount of research was focused on imitating peroxidase activity with Fe_3O_4 MNPs and its potential applications [15-17]. Compared with nature horseradish peroxidase (HRP), Fe_3O_4 MNPs show advantages of high stability at high pH and temperatures, easy preparation and storage, as well as recyclability. However, the affinity of Fe_3O_4 MNPs to substrate is weaker than that of HPR, and Fe_3O_4 MNPs tend to aggregate because of their large surface-area-to-volume ratio, which decreases the catalytic activity. The catalytic activity of Fe_3O_4 MNPs can be increased by ultrasound modification [18-19] and surface coating [20-23]. Mesoporous silica-coated Fe_3O_4 MNPs are highly attractive owing to unique properties of tunable pore size, high porosity and surface area, good chemical stability and easy surface modification [24-25]. High porosity and high surface area

could improve the dissolution kinetics of poorly water-soluble Fe_3O_4 MNPs [26], thereby improving the affinity of Fe_3O_4 MNPs to substrate. Surface modification could enhance the interactions between Fe_3O_4 MNPs and substrate [27]. In addition, mesoporous silica-coated Fe_3O_4 MNPs prevent the aggregation of Fe_3O_4 MNPs and allow small active molecules to diffuse in and out of the mesoporous silica, which lead to increased catalytic activity [28].

β-cyclodextrin (β-CD) is a cyclic oligosaccharide composed of seven D-(+)-glucopyranose units joined by α-(1,4)-linkages. The β-CD structure is a cylindrical cavity, which has the properties of hydrophobic internal cavities and hydrophilic exterior surfaces. This structure can form inclusion complexes with aromatic compounds in their internal cavities by non-covalent binding [29]. In addition, different CD derivatives such as 2-hydroxypropyl-β-CD (HP-β-CD) and methyl-β-CDs can be used to modify the physicochemical and inclusion properties of the host molecules [30]. Therefore, β-CD and its derivatives are often used for molecular recognition and for improving selectivity and sensitivity [31-32].

Herein, we reported that Fe_3O_4@mSiO_2@HP-β-CD mesoporous MNPs (MMNPs) were prepared through a three-step. Fe_3O_4@mSiO_2@HP-β-CD nanoparticles exhibited intrinsic peroxidase-like activity and can catalyse the oxidation of a peroxidase substrate 3,3′,5,5′-tetramethylbenzidine (TMB) by H_2O_2, which causes a colour change. The modification of mesoporous silica onto Fe_3O_4 MNPs and the introduction of HP-β-CD could hinder Fe_3O_4 MNP aggregation, allow small active molecules to diffuse in and out of the mesoporous structure, increase catalytic activity and improve the selectivity. Serving as robust non-reactors, Fe_3O_4@mSiO_2@HP-β-CD can also catalyse the oxidation of β-E_2 in the presence of H_2O_2. A colourimetric sensor based on the catalytic reaction of TMB with H_2O_2 was applied for indirect detection of β-E_2 (Scheme 1).

2. Experimental

2.1. Chemicals and materials

Ferric chloride, ferrous chloride, ammonium hydroxide (25–30 wt%), tetraethylorthosilicate (TEOS), vinyltriethoxysilane, cetyltrimethylammonium bromide (CTAB), sodium citrate, carbodiimide (99.0%), TMB and 30% H_2O_2 were purchased from Guangzhou Chemical Reagent Company (Guangzhou, China). Methacrylic acid (MAA), ethylene glycol dimethyl acrylate (EGDMA), azobisisobutyronitrile (AIBN), Tween 80 and Span 80 were purchased from Aladdin

Co., Ltd. (Shanghai, China). β-E_2 and HP-β-CD were purchased from Sigma-Aldrich. Femoston tablets (license numbers 20110159 and 20110208, Abbott Biologicals B.V.) and estrofem tablets (license numbers X20010081 and 20090307, Novo Nordisk A/S) were purchased from a local drugstore. All other chemicals were of analytical grade. Distilled water was used in all experiments.

2.2. Instruments

Fe_3O_4@mSiO_2@HP-β-CD nanoparticles were characterized by scanning electron microscopy (SEM, Philips SEM-Philips XL-30, and the Netherlands) and Fourier transform infrared spectrometry (FT-IR, NEXUS670, Nicolet, USA). Specific surface area and average pore size of the nanoparticles were measured from nitrogen adsorption data according to the Barrett–Joyner–Halenda and Brunauer–Emmett–Teller methods, respectively, by using an ASAP2020 M+C system (Micromeritics, USA). UV–Vis absorption spectra were recorded on an Australia GBC UV/VIS 916 spectrophotometer. XRD patterns were recorded using a Bruker D8 Advance XRD equipped with Cu Kα radiation (Bremen, Germany). A Thermo Electron inductively coupled plasma atomic emission spectrometer (NexION300X, PerkinElmer, USA) was used for iron determinations. The LC-MS system was used to analyze the reaction product of β-E_2 oxidation and composed by LC-20AT system (Shimadzu Corporation) and a Thermo Fisher Exactive mass spectrometric detector. HPLC analysis was performed on a SPD-20A C_{18} column (150 mm×4.6 mm i.d. 5 μm particle size) (Shimadzu Corporation, Japan). Mobile phase: methol/H_2O containing 0.01% TFA (30:70 ~ 100:0 methol/H_2O). Flow rate: 0.3 mL/min. Injection volume: 10 μL.

2.3. Fe_3O_4@mSiO_2 preparation

Fe_3O_4 MNPs were synthesized by the chemical co-precipitation method. $FeCl_3.6H_2O$ (11.12 g, 0.5 mol) and $FeCl_2 \cdot 4H_2O$ (9.95 g, 0.05 mol) were dissolved in 100 mL of distilled water by stirring, purged with nitrogen gas to displace oxygen for 10 min and heated to 80 ℃ under nitrogen atmosphere. Then, 10 mL of ammonium hydroxide solution (25%) was added into the solution until a pH of 11 was reached. After 1 h, the reaction solution was naturally cooled to room temperature. The obtained black precipitate was separated by a permanent magnet and successively washed with ethanol and distilled water several times. The products were dried in a vacuum oven at 50 °C for 24 h.

Afterward, 50 mg of synthesized Fe_3O_4 particles and 300 mg of CTAB were dispersed in a solution of 100 mL of distilled water, 50 mL of ethanol, and 30 mL of 0.01 mol/L NaOH solution by ultrasonic for 30 min. Approximately, 0.3 mL of TEOS was added dropwise to the mixture with mechanical stirring at 1000 rpm. After 12 h of vigorous stirring at 60 ℃, the black precipitate was isolated with a magnet, washed with distilled water, dried at 50 ℃ and extracted with a mixed solution of 50 mL of 10 mg/mL ammonium nitrate and ethanol solution several times under stirring to remove CTAB. The products were dried at 50 ℃ under vacuum for 24 h.

2.4. Fe_3O_4@mSiO_2@HP-β-CD preparation

Approximately 0.8 g of HP-β-CD was mixed with 25 mL of 0.5 mol/L sodium citrate solution by ultrasonic for 30 min. Then, the mixture was heated to 60 ℃ and stirred at 300 rpm for 12 h. After naturally cooling the reaction solution to room temperature, 10 mL of anhydrous alcohol was added into it to promote flocculation. The precipitate was filtered and washed three times with anhydrous ethanol, dried at 50 ℃, and citric acid-modified HP-β-CD was obtained.

Approximately, 100 mg Fe_3O_4@mSiO_2 was dispersed in a 50 mL of NaH_2PO_4-Na_2HPO_4 phosphate buffer solution (pH 6.0) by ultrasonic for 10 min. Then, 0.5 mL of 0.025 g/mL carbodiimide solution was added into the solution, and the mixture was further ultrasound for 15 min. Subsequently, 0.5 g of citric acid-modified HP-β-CD was added under ultrasonic. After 90 min, the magnetic precipitates were collected by a magnet, washed several times with anhydrous ethanol, and dried at 50 ℃ under vacuum for 24 h.

2.5. H_2O_2 detection using Fe_3O_4@mSiO_2@HP-β-CD as peroxidase-like activity

To investigate the peroxidase-like activity of the as-prepared Fe_3O_4@mSiO_2@HP-β-CD, the catalytic oxidation of the peroxidase substrate TMB in the presence of H_2O_2 was tested. In a typical experiment, 30 μL of 8.3 mM TMB, 50 μL (1.5 mg) of the Fe_3O_4@mSiO_2@HP-β-CD and 20 μL of 0.01 M H_2O_2 were added into 2.9 mL of sodium citric acid−phosphate buffer (pH 4.0) at 40 ℃. After the addition of TMB substrates, colour reactions were immediately observed. To establish the concentration dependence response, H_2O_2 concentration ranged from 0.1 μM to 66.7 μM in reaction mixture. The kinetic parameters of the catalytic reaction were also determined by changing the concentration of TMB and H_2O_2 in this system. The Michaelis–Menten constant was calculated using the Lineweaver–Burk plots of the double reciprocal of the Michaelis–Menten equation, $1/\nu = K_m/V_{max}(1/[S])+1/V_{max}$, where ν is the initial velocity, V_{max} is the maximum

reaction velocity, [S] is the concentration of the substrate, and K_m is the Michaelis constant.

2.6 Sample preparation

Poultry feed samples were purchased from a feed corporation. Approximately 5 g of feed sample was weighed into a 50 mL plastic centrifuge tube, and 20 mL of acetone were added. After vortexing for 2 min, the mixture was sonicated for 30 min and then centrifuged at 4,000 rpm for 15 min. The supernatant was filtered through 0.22 μm membrane and transferred to another glass tube. The solid layer was extracted once again with 20 mL of acetonitrile. The extracts were combined and evaporated to dry under N_2 at 60 ℃. The residue was dissolved in 1.00 mL of acetone for further molecularly imprinted solid-phase extraction (MISPE).

A total of 10 β-E_2 tablets (Femoston) were powdered. An amount of this powder corresponding to one tablet of β-E_2 content was weighed into a 50 mL plastic centrifuge tube. After adding 20 mL of acetone, the mixture was sonicated for 30 min and then centrifuged at 4,000 rpm for 15 min. The supernatant was transferred to 250 mL calibrated flask. The solid layer was extracted once again with 20 mL of acetone. The extracts were combined to 250 mL calibrated flask and filled to volume with acetonitrile for further MISPE.

2.7. MISPE procedure and β-E_2 detection

β-E_2 molecular imprinted polymer was synthesized using a method described by Wang et al [33]. The cartridges were prepared by packing 300 mg of the dry imprinted polymer into empty SPE-cartridges (Supelco, USA). The cartridges were preconditioned with 3 mL of methanol–acetic acid (9:1, v/v), 3 mL of methanol, and 3 mL of acetone successively. The sample (1.0 mL) obtained after extraction were loaded onto the cartridges with the speed of 1 mL·min^{-1}. After loading, the cartridges were washed with 4 mL of 20% acetone and centrifuged at 4000 rpm for 5 min. Finally, the extracts were eluted with 2 mL of methanol−1 M HCl (1:1, v/v) with the speed of 0.2 mL·min^{-1}. The elution was immediately dried at 60 ℃ under a nitrogen stream. The residue was dissolved in 2.97 mL of sodium citric−phosphate buffer (pH 4.0) containing of 50 μL (1.5 mg) Fe_3O_4@mSiO_2@HP-β-CD and 20 μL of 0.01 M H_2O_2 for incubation at 40 ℃ for 20 min. Then, 30 μL 8.3 mM TMB was added. The resulting solution was mixed and incubated for 20 min at 40 ℃. Next, the Fe_3O_4@mSiO_2@ HP-β-CD was removed from the reaction solution by an external magnetic field. Finally, the reaction solution was used to perform the adsorption spectroscopy measurement.

3. Results and discussion

Scheme 2 of the two reactions depicts the principle of the colourimetric sensor for β-E_2 detection based on the peroxidase-like activity of Fe_3O_4@mSiO_2@HP-β-CD. β-E_2 oxidation was catalysed by Fe_3O_4@mSiO_2@HP-β-CD nanocomposites in the presence of excessive and quantitative H_2O_2. The UV spectra (Fig. S1) results showed that β-E_2 has been removed from reaction solution. The reaction product of β-E_2 oxidation was analyzed by LC-MS. The LC-MS analytical results (Fig. S2) showed that the reaction product of β-E_2 oxidation was mainly (7a-Methyl-1-oxo-2,3,3a,6,7,7a-hexahydro-1H-inden-4-yl)-acetaldehyde and 4-(2-Hydroxy–ethyl)-7a-methyl-octahydro-indene-1,5-diol. Moreover, excessive H_2O_2 was quantitatively used to oxidize peroxidase substrate TMB to form a blue product (oxidized TMB) in the presence of Fe_3O_4@mSiO_2@HP-β-CD nanocomposites. Thus, a sensitive colourimetric sensor for β-E_2 detection was established by coupling these two reactions by using Fe_3O_4@mSiO_2@HP-β-CD nanocomposites as catalyst and estimating the β-E_2 concentration with the colour change in oxTMB.

3.1. Fe_3O_4@mSiO_2 and Fe_3O_4@mSiO_2@HP-β-CD characterizations

FT-IR is widely used in the structure of organic material studies. The FT-IR spectra of Fe_3O_4 (a), Fe_3O_4@mSiO_2 (b) and Fe_3O_4@mSiO_2@HP-β-CD (c) nanocomposites are shown in Fig. 1. The strong absorption band at 580 cm^{-1} is the Fe−O vibration of the Fe_3O_4 particles. In Figs. 1b and 1c, the characteristic peaks at 1085 and 1091 cm^{-1} correspond to the Si−O−C and Si−O−Si stretching vibrations, respectively. The peaks at 966, 1640 and 3439 cm^{-1} indicate the −OH vibration from H_2O and Si−OH or HP-β-CD [34]. The peaks at 1384, 2933, 1497 and 2850 cm^{-1} were attributed to the C−H vibrations of CH_3 and CH_2 from TEOS. Compared with the peak intensity of Fe−O at 580 cm^{-1}, Fe_3O_4@mSiO_2 and Fe_3O_4@mSiO_2@HP-β-CD had very weak Fe−O vibration, which indicated that SiO_2 had been successfully coated on the Fe_3O_4 surface. Compared with the infrared data of Fe_3O_4@mSiO_2, the absorption of Fe_3O_4@mSiO_2@HP-β-CD at 3431, 1085 cm^{-1} corresponding to Fe_3O_4@mSiO_2 showed a little drift and wide variation. At the same time, the stretching vibrations of the –CH_3 groups at 1384cm^{-1} disappeared. The result indicates that HP-β-CD has been successfully immobilized on the Fe_3O_4@mSiO_2 surface.

The XRD pattern of the Fe_3O_4 (a), Fe_3O_4@mSiO_2 (b) and Fe_3O_4@mSiO_2@HP-β-CD (c) is shown in Fig. 2. It could be seen in Fig. 2a that the diffraction angles at 2θ value about

18.3°, 30.2°, 35.6°, 43.3°, 53.6°, 57.2°, and 62.8° corresponded to the cubic phase of Fe_3O_4 (1 1 1), (2 2 0), (4 0 0), (4 2 2), (5 1 1), and (4 4 0), which could be indexed to the Fe_3O_4 phase. After being coated by SiO_2, the diffraction peaks of Fe_3O_4 are also observed as shown in Fig. 2b, but the intensity of corresponding peaks decreased obviously, moreover a wide diffraction between 15 and 28 of 2θ values of SiO_2 could be found. This shows that SiO_2 is amorphous phase [35]. Compared with Fig. 2b, the diffraction peaks of Fe_3O_4 and SiO_2 are also observed for the Fe_3O_4@mSiO_2@HP-β-CD in Fig. 2c, but the intensity of the peaks related to the above two figures was further attenuated because of HP-β-CD coated. The result further confirms the coating of SiO_2 on Fe_3O_4 and HP-β-CD on Fe_3O_4@SiO_2.

To know the loading of Fe_3O_4 in each sample, ICP-MS was performed. The determined mean values (n=3) for Fe_3O_4 were 17.07% and 4.98% in Fe_3O_4@mSiO_2 and Fe_3O_4@mSiO_2@HP-β-CD sample, respectively.

SEM images of the morphological features of Fe_3O_4@mSiO_2 and Fe_3O_4@mSiO_2@HP-β-CD are shown in Fig.3. The Fe_3O_4@mSiO_2 (Figs. 3a and 3c) and Fe_3O_4@mSiO_2@ HP-β-CD (Figs. 3b and 3d) were spherical with a rough surface, displayed good dispersion and consisted of mesh units. The particle sizes of Fe_3O_4@mSiO_2@HP-β-CD and Fe_3O_4@mSiO_2 were estimated to be about 150 and 40 nm, respectively. The specific surface area, average pore diameter and pore volume of Fe_3O_4@mSiO_2@HP-β -CD and Fe_3O_4@mSiO_2, determined by nitrogen sorption, are summarized in Table 1. The surface areas and average pore diameter of Fe_3O_4@mSiO_2 decreased with HP-β-CD modification.

3.2. Peroxidase-Like Activity of Fe_3O_4@mSiO_2@HP-β-CD

Peroxidase can catalyse TMB oxidation to produce a blue colour reaction. Therefore, the peroxidase-like activity of Fe_3O_4@mSiO_2@HP-β-CD was investigated using TMB as peroxidase substrate in the presence and absence of H_2O_2. As expected in Fig. 4, Fe_3O_4@mSiO_2@ HP-β-CD could catalyse the oxidation of TMB in the presence H_2O_2 to produce the typical blue colour reaction. The maximum absorbance of the reaction was 652 nm, which came from the oxidation products of TMB. A negligible blue colour was found in the absence of H_2O_2, indicating no oxidation reaction with TMB and Fe_3O_4@mSiO_2@HP-β-CD. Furthermore, a light blue was observed in the presence of only TMB and H_2O_2, showing that TMB could be oxidized by H_2O_2 in the absence of any catalyst under our conditions, such as that observed in early works [36-37].

However, the Fe_3O_4@$mSiO_2$@ HP-β-CD has higher response for the TMB oxidation by H_2O_2, which is similar to HRP. The results confirmed that Fe_3O_4@$mSiO_2$@HP-β-CD has peroxidase-like catalytic activity in the absence of any other catalysts.

To investigate the functions of HP-β-CD in the peroxidase-like activity of Fe_3O_4@$mSiO_2$@HP-β-CD nanocomposites, the catalytic activity of Fe_3O_4@$mSiO_2$@HP-β-CD was compared with that of Fe_3O_4@$mSiO_2$ under the same conditions for 30 min (Fig. 5). The oxidation rate of TMB by H_2O_2 with Fe_3O_4@$mSiO_2$@HP-β-CD as catalyst was significantly faster than that of Fe_3O_4@$mSiO_2$. The absorbance of the Fe_3O_4@$mSiO_2$@HP-β-CD system at 652 nm was higher than that of Fe_3O_4@$mSiO_2$ system. The results indicated that HP-β-CD modification on the surface of Fe_3O_4@$mSiO_2$ can effectively improve peroxidase-like activity.

3.3. Optimization of experimental conditions

To acquire a high catalytic efficiency, the experimental conditions including pH of reaction solution, incubation temperature and time and amount of catalyst were investigated. As seen in Figs. 6 (A and B), the catalytic activity increased when the pH increased from 2.0 to 4.0 and temperature increased from 5 ℃ to 40 ℃, and then decreased. The optimal pH and temperature were pH 4.0 and 40 ℃, respectively. The catalytic oxidation of Fe_3O_4@$mSiO_2$@HP-β-CD is faster in acidic solutions than in neutral or basic solutions. This rate is similar to many other peroxidase-like nanomaterials [36-37]. In addition, the incubation time and amount of Fe_3O_4@$mSiO_2$@HP-β-CD were also studied. As seen in Figs. 6 (C and D), the absorbance increased when the incubation time was in the range of 5 min to 20 min, and the Fe_3O_4@$mSiO_2$@HP-β-CD' weight was in the range of 0.25 mg−1.5 mg, after which had a slight decrease. This result is due to the increasing amount of active sites with the increase of the amount of catalyst, and the slight decrease of the absorbance may be attributed to the agglomeration of microspheres and the scavenging of ·OH by excess Fe^{2+} [38]. The optimal reaction time and amount of catalyst were 20 min and 1.5 mg, respectively.

For a given concentration of TMB (83.2 μM), the catalytic activity of the Fe_3O_4@$mSiO_2$@HP-β-CD was H_2O_2 concentration dependent. Fig. 7 (A) shows a typical H_2O_2 concentrations response curve. The absorbance linearly increased when H_2O_2 concentrations increased up to 1.0 mM. However, further increases in concentration did not significantly increase the catalytic efficiency because of the complete oxidation of TMB in the reaction system. The

system discussed above could be developed to determine H_2O_2. The absorbance at 652 nm was linear to H_2O_2 concentrations ranging from 1.06×10^{-6} mol·L^{-1} to 1.0×10^{-4} mol·L^{-1} with a detection limit (S/N=3) of 3.0×10^{-7} mol·L^{-1} (Fig. 7 B). The linear equation was A=0.0208 + 7492.05c (mol·L^{-1}), with a correlation coefficient of 0.995. The relative standard deviation (RSD) for 6.7×10^{-5} mol·L^{-1} was 2.0% (n = 6).

To investigate the reusability of the Fe_3O_4@mSiO_2@HP-β-CD under optimal condition, a catalyst was used in the catalytic for 10 cycles. A magnet was used to collect the catalysts, which were then washed with distilled water before the succeeding cycle. As shown in Fig. 8, the catalytic activity of Fe_3O_4@mSiO_2@HP-β-CD remained 86% after five cycles. It may be attributed to the loss and agglomeration of Fe_3O_4@mSiO_2@HP-β-CD by washing with distilled water before the succeeding cycle. Although the catalytic activity of Fe_3O_4@mSiO_2@HP-β-CD slowly decreased, but after 10 cycles, the catalytic activity of Fe_3O_4@mSiO_2@HP-β-CD still remained 63%, indicating that Fe_3O_4@mSiO_2@ HP-β-CD had good reusability and stability and can meet the requirement for practical application.

3.4. Steady-state Kinetic Analysis of Fe_3O_4@mSiO_2@HP-β-CD

The peroxidase-like catalytic property of Fe_3O_4@mSiO_2@HP-β-CD nanocomposites was further investigated by determining the apparent steady-state kinetic parameters of the catalytic reaction. A series of initial rates were calculated based on the molar absorption coefficient of TMB-derived oxidation products (ε_{650nm} = 3.9×10^4 mol·L^{-1} cm^{-1}) from the absorbance (650 nm, vs. time plots) by changing the concentration of TMB and H_2O_2 in this system [39]. As shown in Fig. 9, typical Michaelis−Menten curves were obtained for Fe_3O_4@mSiO_2@HP-β-CD with both TMB and H_2O_2. The reciprocal of initial rate was proportional to the reciprocal of substrate (TMB and H_2O_2) concentration, indicating that the reaction followed the Michaelis−Menten behaviour. The Michaelis−Menten apparent constant (K_m) and maximum initial velocity (V_{max}) were obtained using Lineweaver-Burk plot (Table 2). According to previous reports [36–39], when the value of K_m is small, the affinity between the enzyme and the substrate is strong and the catalyst is efficient. The K_m value of Fe_3O_4@mSiO_2@HP-β-CD was remarkably lower than that of HRP for H_2O_2 and TMB, indicating that the Fe_3O_4@mSiO_2@ HP-β-CD exhibited higher affinity than HRP for H_2O_2 and TMB. The reason could be that the modification of mesoporous silica onto Fe_3O_4 MNPs allows H_2O_2 to diffuse in and out of the mesoporous, and the introduction of HP-β-CD could form

inclusion complexes with TMB. Similarly, the K_m value of Fe_3O_4@$mSiO_2$ @HP-β-CD with H_2O_2 as the substrate was significantly lower than that of Fe_3O_4 NP alone, showing that Fe_3O_4@$mSiO_2$ @HP-β-CD had higher affinity for H_2O_2 than Fe_3O_4 NP alone. However, the K_m value of Fe_3O_4@$mSiO_2$ @HP-β-CD with TMB was similar to that of Fe_3O_4 NP alone. These results revealed that the as-prepared Fe_3O_4@$mSiO_2$@HP-β-CD possessed high peroxidase-like activity.

3.5. Detection of β-E_2 using the Fe_3O_4@SiO_2@ HP-β-CD for peroxidase-like

Given that Fe_3O_4@$mSiO_2$@HP-β-CD can catalyse the oxidation of β-E_2 in the presence of H_2O_2, the combination of the catalytic reaction of TMB with H_2O_2 and colourimetric sensor for indirect detection of β-E_2 was investigated. The typical β-E_2 concentration−response curves shows in Fig. 10. The colour variations in TMB oxidation catalysed by Fe_3O_4@$mSiO_2$@HP-β-CD nanocomposites were β-E_2 concentration dependent, the absorbance linearly decreased when the concentration of β-E_2 over the range of 0.8 μM to 16.0 μM, indicating that the absorbance change could be used to detect β-E_2. The calibration equation in aqueous solution was A=0.631−0.0232c (μM), with a correlation coefficient (r) of 0.997. The detection limit in aqueous is 0.2 μM. Different amounts of β-E_2 were added to 5 g of blank feed sample to eliminate the interference of matrix; the corresponding final concentrations of β-E_2 were 0.8, 1.6, 3.2, 6.4, 9.6, 12.8 and 16 μM. Feed spiked samples were treated as the steps described in the Sections 2.6 and 2.7. The obtained calibration equation in feed extract was A=0.598−0.0225c (μM, r=0.995) for feed. No significant differences were observed of the calibration curve for β-E_2 in aqueous and in matrix. The results showed that the matrix could be efficiently removed during the sample extraction and MISPE preconcentration stage. The detection limit in feed is 0.033 mg·kg^{-1} (0.2 μM), which is similar to reports from Jiang using MISPE-HPLC method in fish (0.023 mg·L^{-1}) [41] and is more sensitive than that Yilmaz reported using UV spectrophotometry in tablets (0.15 mg·L^{-1}) [5]. Thus, this developed method is sensitive enough to determine the β-E_2 in tablets and feed.

3.6. Interference and Selectivity

To investigate the selectivity of the method, interference experiments were performed with 10 times concentration of interference encountered from the common tablet excipients and feed, such as talc, gelatine, lactose, starch, protein, fat, phosphorus, calcium, magnesium stearate, titanium dioxide, methyl hydroxypropyl cellulose, lysine, methionine, indigotin, estrone and dydrogesterone. The talc, gelatine, lactose, starch, fat, phosphorus, calcium, magnesium stearate

and titanium dioxide did not interfere with the determination of β-E_2. However, 10 times concentration of protein, methyl hydroxypropyl cellulose, lysine, methionine, indigotin, estrone and dydrogesterone were in place of β-E_2, and the colour difference could not be distinguished by the naked eye, showing that these excipients interfered with the determination of β-E_2. Protein, methyl hydroxypropyl cellulose and indigotin can be removed by organic solvent precipitation and 0.22 μm filter membrane in sample extraction (Section 2.6). Lysine, methionine, estrone and dydrogesterone can be effectively eliminated through the leaching step of MISPE by using 4 mL of 20% acetone (Sections 2.6 and 2.7). Therefore, it is possible to determine β-E_2 in commercial tablet and feed sample with high accuracy by combining with MISPE sample pretreatment.

3.7. Precision and accuracy

The precision and accuracy of the overall procedure were evaluated by analysing the femoston tablets (license number 20110159, 0.1468 g/per white tablet) containing 1 mg β-E_2 and a blank feed sample, spiked with β-E_2 at three different concentrations (Sections 2.6 and 2.7) and six replicates. The precision and accuracy were expressed as the relative standard deviation (RSD) and recovery, respectively. As shown in Table 3, the determined mean values were 6.6 ± 0.2 $mg \cdot g^{-1}$ for β-E_2 in white tablets, which were coincident with the corresponding labelled values 6.8 $mg \cdot g^{-1}$. The RSD was 3.0%. The recoveries obtained and RSD from the spiked tablets ranged from 94.0% to 102% and from 2.5% to 3.2% respectively. These results indicated that the method had good precision and accuracy.

3.8. Application

To demonstrate the application of the method, two estrofems (license numbers 20090307 and X20010081), two femostons (license numbers 20110208 and X20110159) and four feed samples (Sections 2.6 and 2.7) were analysed. The results are shown in Table 4.The β-E_2 in the four feed samples was not detected. After the strict control of the administrative agency, the illegal usage of β-E_2 seemed to be rare. Recoveries of β-E_2 from the two estrofems (20090307 and X20010081) and two femostons (20110208 and X20110159) ranged from 92.6% to 110% with RSD > 5.4%, which is consistent with that labelled value of tablet samples.

4. Conclusion

In this paper, Fe_3O_4@mSiO_2@HP-β-CD nanocomposites were synthesised and investigated for peroxidase-like activity. The Fe_3O_4@mSiO_2@HP-β-CD nanocomposites exhibited Michaelis–

Menten kinetics and higher catalytic activity than Fe_3O_4@$mSiO_2$ without HP-β-CD functionalization. A simple, selective colourimetric method for H_2O_2 detection was developed based on the Fe_3O_4@$mSiO_2$@HP-β-CD−TMB−H_2O_2 system. A detection limit of as low as 3×10^{-7} mol·L^{-1} can be obtained. More importantly, an economical, visual method for daily monitoring of β-E_2 in commercial tablets and feeds was fabricated using this system coupled with MISPE sample pre-treatment. Good precision and good accuracy were obtained for the detection of β-E_2 in commercial tablets and spiked feeds. The developed method demonstrates the potential of Fe_3O_4@$mSiO_2$@HP-β-CD nanocomposites as novel peroxidase-like enzyme for various applications, such as pharmaceutical preparation, raw material formulation, food safety, biochemistry, and catalysis.

Acknowledgements

This work is financially supported by the Science and Technology Planning Project of Zhaoqing City, Guangdong province (no. 2013C019 and no. 2015B010301002), the Science and Technology Innovation Project of Guangdong provincial education department (no. 2012kjcx0104), and the Characteristic Innovation Project of Education Department of Guangdong Province (no. 2014ktscx192).

References

[1] L.Havlikova, L.Novakova, L. Matysova, J. Sicha , P. Solich, *J. Chromatogr. A*, 2006, **1119,** 216.

[2] D. Arroyo, M.C. Ortiz, L.A. Sarabia, *J. Chromatogr. A,* 2007, **1157**, 358.

[3] G. Ferretti, C. Ferranti, T. Crovella, M. Fiori, C. Civitareale, C. Marchiafava, F. D. Quadri, P. Cammarata, L. Palleschi, *J. Chromatogr. B*, 2008, **871**, 135.

[4] L. Nygaard, H.D. Kilde, S.G. Andersen, L. Henriksen, V. Overby, *J. Pharmaceut. Biomed. Anal.*, 2004, **34**, 265.

[5] B. Yilmaz, Y. Kadioglu, *Arab. J. Chem.,* doi:10.1016/j.arabjc.2013.04.018

[6] B. Salci, I. Biryol, *J. Pharmaceut. Biomed. Anal.*, 2002, **28**, 753.

[7] Feng Long, Hanchang Shi and Hongchen Wang，*RSC Adv.*, 2014, **4**, 2935.

[8] E. Leal, E. Sánchez, B. Muriach, *J. Comp. Physiol. B*, 2009, **179**, 77.

[9] L. Z. Gao, J. Zhuang, L. Nie, J.B. Zhang, Y. Zhang, N. Gu, T.H. Wang, J. Feng, D.L. Yang, S. Perrett, X.Y. Yan, Nat. *Nanotechnol.*, 2007, **2**, 577.

[10] H. Wei, E.K. Wang, *Anal. Chem.,* 2008, **80**, 2250.
[11] S. Wang, W. Chen, A.L. Liu, L. Hong, H.H. Deng, X.H. Lin, *Chemphyschem*., 2012, **13**, 1199.
[12] F. Pogacean, C. Socaci, S. Pruneanu, A. R. Biris, M. Coros, L. Magerusan, G. Katona, R. Turcu, G. Borodi , *Sensor. Actuat. B*, 2015, **213**, 474.
[13] W. Zhu, J. Zhang, Z. Jiang, W. Wang, X. Liu, *RSC Adv.*, 2014, **4**, 17387**.**
[14] H. Wei, E. Wang, *Chem. Soc. Rev*.**,** 2013, **42,** 6060.
[15] Z. Can, A. Üzer, K. Türkekul, E. Erçağ, R. Apak, *Anal. Chem.*, 2015, **87(19)**, 9589.
[16] N. Ding, N. Yan, C. Ren, X. Chen, *Anal. Chem*., 2010, **82**, 5897.
[17] S.H. Liu, R. Lu, R.M. Xing, J.J. Zhu, *Chem.−Eur. J*., 2011, **77**, 620.
[18] N. Wang, L. Zhu, D. Wang, M. Wang, Z. Lin, H. Tang, *Ultrason. Sonochem*., 2010, **17**, 526.
[19] N. Wang, L. Zhu, M. Wang, D. Wang, H. Tang, *Ultrason. Sonochem*., 2010, **17**, 78.
[20] Xiaochen Wu, Yan Zhang, Ting Han, Haixia Wu, Shouwu Guo and Jingyan Zhang, *RSC Adv.*, 2014, **4**, 3299.
[21] M. Yang , Y. Guan, Y. Yang, T. Xia, W. Xiong, N. Wang, C. Guo, *J. Colloid Interf. Sci*., 2013, **405**, 291.
[22] Hui Wang, Huan Jiang, Sha Wang, Wenbing Shi, Jianchuan He, Hong Liu and Yuming Huang, *RSC Adv.*, 2014, **4**, 45809.
[23] Y. Long, M. Xie, J. Niu, P. Wang, *J. Ma, Appl. Surf. Sci*., 2013, **277**, 288.
[24] P. Kuhn, A. Thomas, M. Antonietti, *Macromolecules*, 2009, **42**, 319.
[25] S. Xuan, F. Wang, J.M.Y. Lai, K.W.Y. Sham, Y.J.Wang, S.F. Lee, J.C. Yu, C.H.K. Cheng, K.C.F. Leung, *ACS Appl. Mater. Inter.,* 2011, **3**, 237.
[26] Y. Zhang, J. Zhang, T. Jiang, S. Wang, *Int. J. Pharm.*, 2011, **410**, 118.
[27] J.M. Rosenholm, M. Lindén, *J. Control Release*, 2008, **128**, 157.
[28] Y. Wang, B. Zhou, S. Wu, K. Wang, X. He, *Talanta*, 2015, **134**, 712.
[29] H.M. Liu, C.H. Liu, X.J. Yang, S.J. Zeng, Y.Q. Xiong, W.J. Xu, *Anal. Chim. Acta*, 2007, **628**, 87.
[30] M. Uzqueda, C. Martín, A. Zornoza, M. Sánchez, M. C. Martínez-Ohárriz, I. Vélaz, *Pharm. Res*., 2006, **23(5)**, 980.
[31] W. Lian, J. Huang, J. Yu, X. Zhang, Q. Lin, X. He, X. Xing, S. Liu, *Food Control*, 2012, **26**,

620.

[32] H. Zhao, X. Ji, B. Wang, N. Wang, X. Li, R. Ni, J. Ren. *Biosens. Bioelectron*., 2015, **65**, 23.

[33] S. Wang, Y. Li, M. Ding, X. Wu, J. Xu, R. Wang, T. Wen, W. Huang, P. Zhou, K. Ma, X. Zhou, S. Du, *J. Chromatogr. B*, 2011, **879**, 2595.

[34] X. Luo, S. Luo, Y. Zhan, H. Shu, Y. Huang, X. Tu, *J. Hazard. Mater*., 2011, **92**, 949.

[35] Z. H. Wang, S. Y. Zhu, S. P. Zhao, H. B. Hu, *J. Alloy. Compd.*, 2011, **509,** 6893.

[36] Q. Liu, H. Li, Q. Zhao, R. Zhu, Y. Yang, Q. Jia, B. Bian, L. Zhuo, *Mater. Sci. Eng. C*, 2014, **41**, 142.

[37] L. Su, J. Feng, X. Zhou, C. Ren, H. Li, X. Chen, *Anal. Chem*., 2012, **84**, 5753.

[38] L.J. Xu, J.L.Wang, *J. Hazard. Mater*., 2011, **186**, 256.

[39] X. Zhang, S. Gong, Y. Zhang, T. Yang, C. Wang, N. Gu, *J. Mater. Chem*., 2010, **20**, 5110.

[40] L. Lin, X. Song, Y. Chen, M. Rong, T. Zhao,Y. Wang, Y. Jiang, X. Chen, *Anal. Chim. Acta*, 2015, **869**, 89.

[41] T. Jiang，L. Zhao，B. Chu，Q. Feng，W. Yan，J.M. Lin, *Talanta*, 2009, **78**, 442.

Table 1 Characteristics of the porous structure of the Fe_3O_4@$mSiO_2$ and Fe_3O_4@$mSiO_2$@HP-β-CD

Sample	The specific surface area ($m^2\ g^{-1}$)	Average pore diameter (nm)	Pore Volumes ($m^2\ g^{-1}$)
Fe_3O_4@$mSiO_2$	584.2	2.6	0.92
Fe_3O_4@$mSiO_2$@HP-β-CD	350.4	1.7	0.59

Table 2 Comparison of the apparent Michaelis−Menten constant (K_m) and maximum reaction rate (V_m)

Catalyst	K_m [mM]		V_m [10^{-8} M s^{-1}]	
	TMB_{fix}	H_2O_{2fix}	TMB	H_2O_2
HRP [9]	0.434	3.70	10	8.71
HRP [40]	0.18	2.39	0.29	4.36
Fe_3O_4 [9]	0.098	154	3.44	9.78
Fe_3O_4@$mSiO_2$@HP-β-CD	0.086	0.414	5.4	5.26

Table 3 Precision and accuracy of β-E_2 tablets (n= 6)

sample	Labeled value ($mg\cdot g^{-1}$)	Found[a] ($mg\cdot g^{-1}$)	Spiked ($mg\cdot g^{-1}$)	Found ($mg\cdot g^{-1}$)	Recovery (%)	RSD (%)
Femoston			5.0	11.3 ± 0.3	94.0	2.7
White tablet	6.8	6.6 ± 0.2	10.0	16.2 ± 0.4	96.0	2.5
			15.0	21.9 ± 0.7	102	3.2
Fish feed			0.50×10^{-3}	$(0.46 \pm 0.02)\times10^{-3}$	92.0	4.3
	–	ND	1.0×10^{-3}	$(0.95 \pm 0.02)\times10^{-3}$	95.0	3.2
			2.0×10^{-3}	$(1.86 \pm 0.05)\times10^{-3}$	93.0	2.7

"–" : No labeled vaule; ND: not detected; [a] Found was expressed with the mean ± standard deviation (SD).

Table 4 Measurement results of β-E2 in different samples（n=3）

Samples	labeled value (mg· g^{-1})	Found (mg· g^{-1})	Recovery (%)	RSD (%)
Estrofem (20090307)	6.8	6.3 ± 0.3	92.6	4.8
Estrofem (X20010081)	6.8	6.5 ± 0.2	95.6	3.1
Femoston (H20110208) white tablets	6.8	6.4 ± 0.3	94.1	4.7
Femoston (H20110208) grey tablets	6.9	7.4 ± 0.4	107	5.4
Femoston (H20110159) white tablets	6.8	6.6 ± 0.2	97.1	3.0
Femoston (H20110159) grey tablets	6.9	7.6 ± 0.4	110	5.3
Shell beans feed	–	ND		
Corn feed	–	ND		
Fish feed	–	ND		
Formula feed	–	ND		

“–” : No labeled vaule; ND: not detected

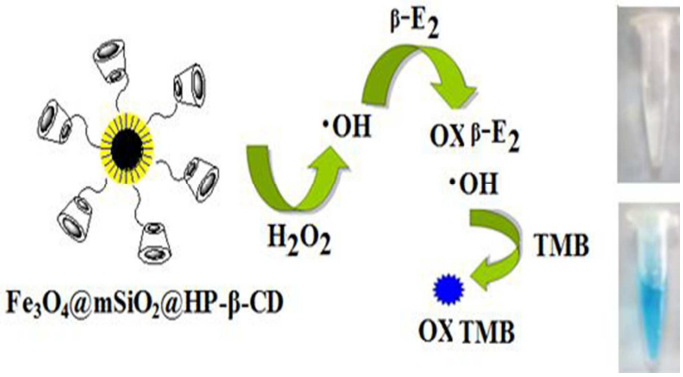

Scheme 1 Schematic illustration of colourimetric detection of β-E_2 by using Fe_3O_4@$mSiO_2$@ HP-β-CD nanoparticles catalyzed color reaction.

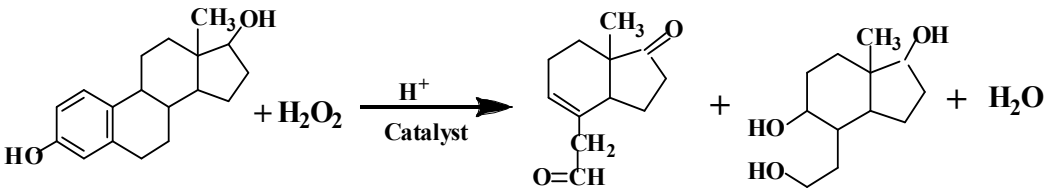

Scheme 2 Colourimetric sensor for β-E_2 detection using Fe_3O_4@mSiO_2@HP-β-CD as catalyst

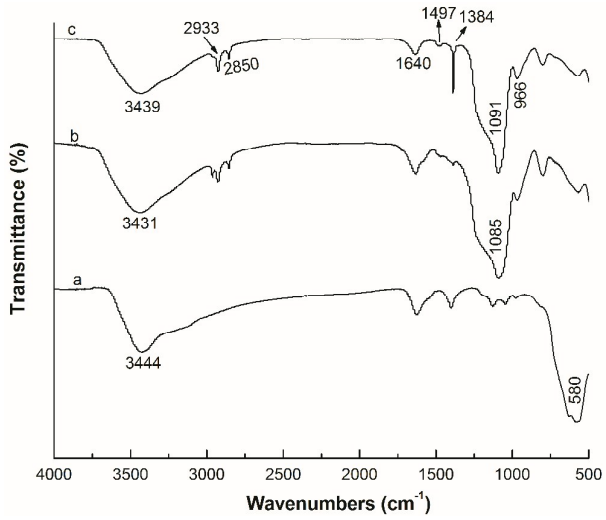

Fig.1. FT-IR spectras of Fe_3O_4 (a), Fe_3O_4@m SiO_2 (b), and Fe_3O_4@m SiO_2@HP-β-CD (c)

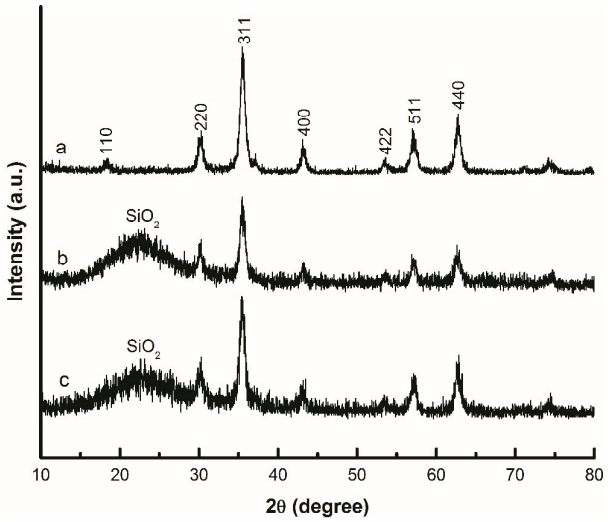

Fig.2. XRD patterns of Fe_3O_4(a), Fe_3O_4@mSiO_2 (b) and Fe_3O_4@mSiO_2@HP-β-CD (c).

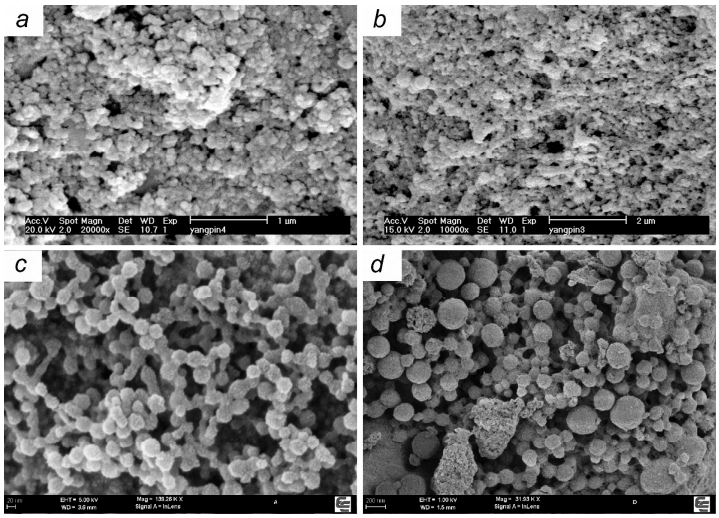

Fig.3 Scanning electronmicrographs of Fe_3O_4@mSiO_2 (a, c) and Fe_3O_4@m SiO_2@HP-β-CD (b, d)

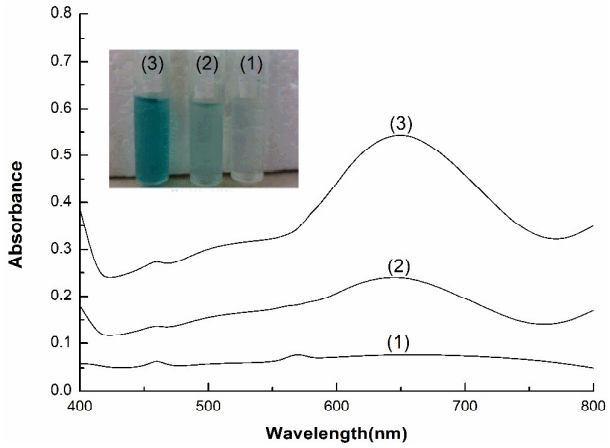

Fig.4 Absorption spectra of different TMB reaction solutions after incubated in pH 4.0 buffer at 40℃for 60 min; (1) TMB+Fe_3O_4@$mSiO_2$@HP-β-CD; (2) TMB+H_2O_2; (3) TMB+H_2O_2+ Fe_3O_4@ $mSiO_2$ @HP-β-CD

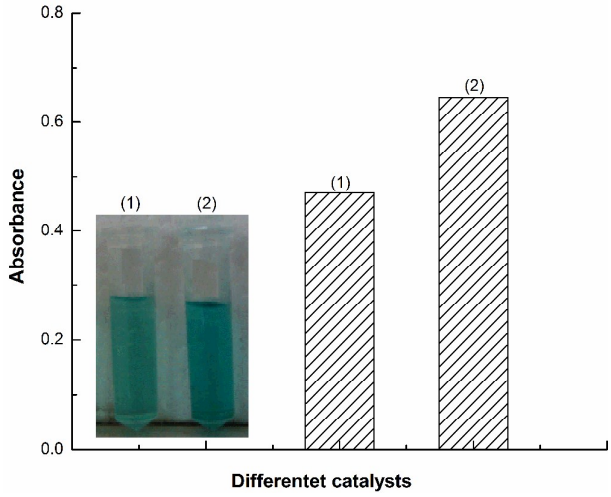

Fig.5 Effect of different catalyst on the TMB reaction solutions in pH 4.0 buffer at 40℃for 30 min; (1) TMB+H_2O_2+ Fe_3O_4@$mSiO_2$; (2) TMB+H_2O_2+ Fe_3O_4@$mSiO_2$@HP-β-CD

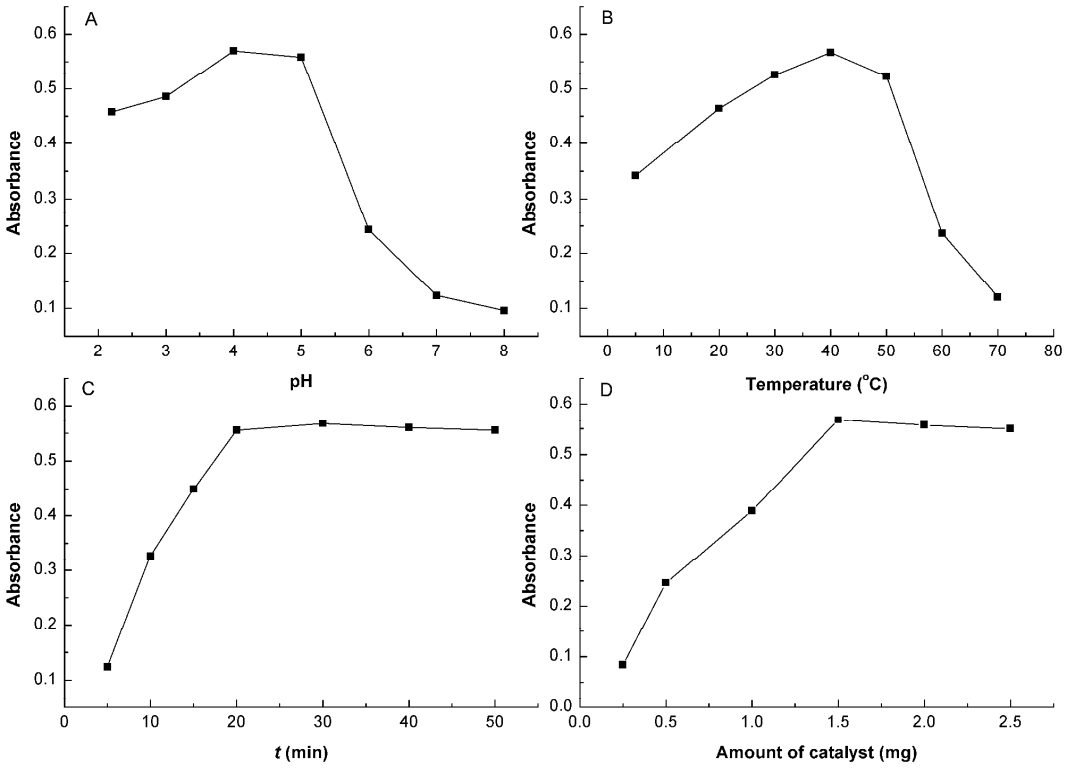

Fig. 6 The effect of pH (A), incubation temperature (B), reaction time (C), and amount of catalyst (D) on the catalytic activity of Fe_3O_4@mSiO_2@HP-β-CD

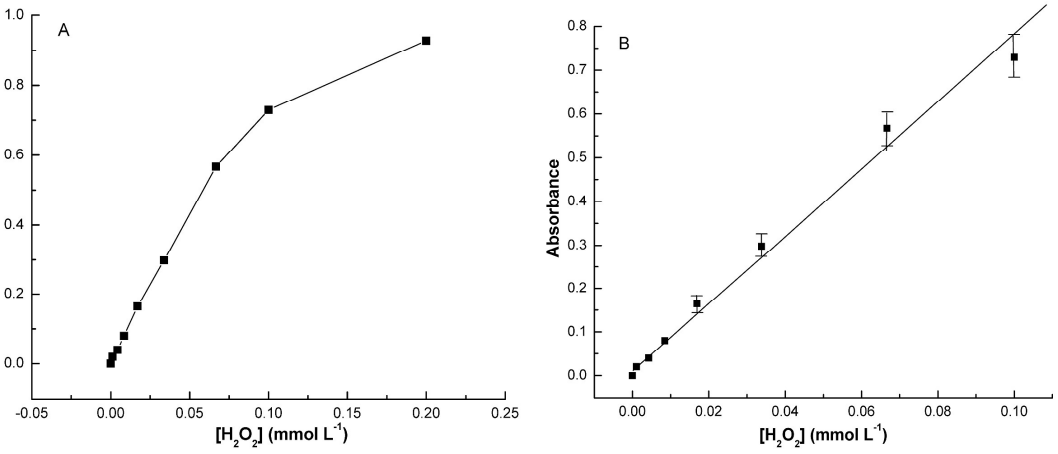

Fig. 7 (A) A dose-response curve for H_2O_2 detection using the Fe_3O_4@mSiO_2@HP-β-CD as artificial enzymes and (B) the linear calibration plot for Fe_3O_4@mSiO_2@HP-β-CD. The error bars represent the standard deviation of three measurements.

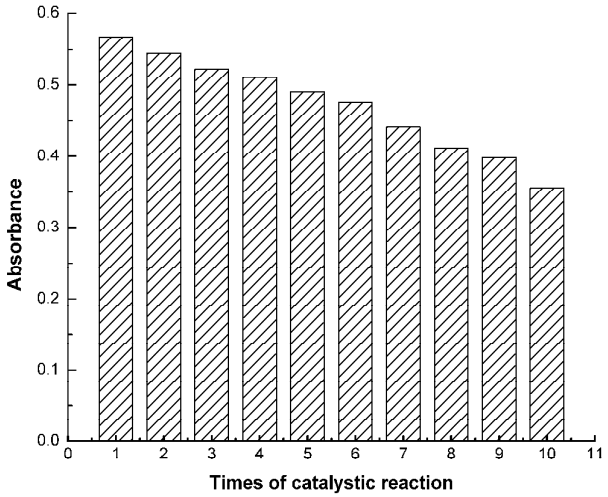

Fig.8 Reusability of Fe_3O_4@mSiO_2@HP-β-CD

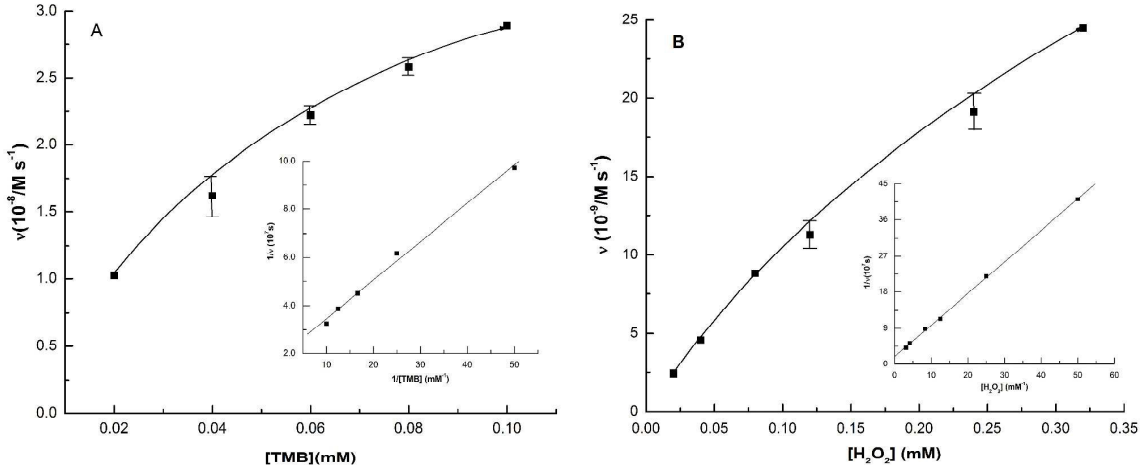

Fig.9 Steady-state kinetic analysis of Fe_3O_4@SiO_2@HP--β-CD. (A) 0.01 M H_2O_2 and different concentration of TMB; (B) 8.32 mM TMB and different concentration of H_2O_2.

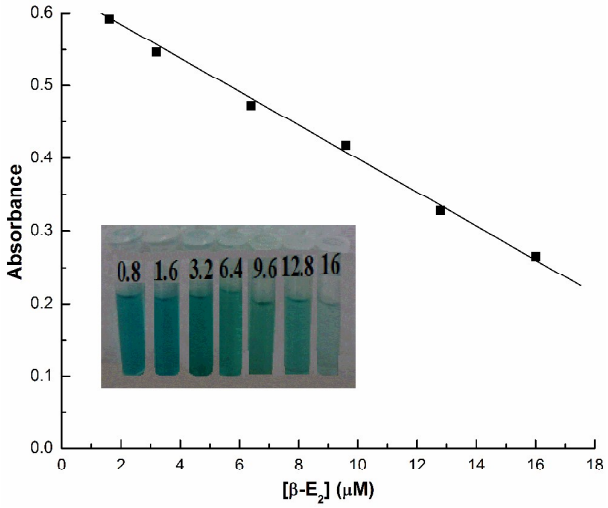

Fig. 10 Typical linear plot of different concentrations of β-E_2 (μM) standard solution under optimal condition

A table of contents entry:

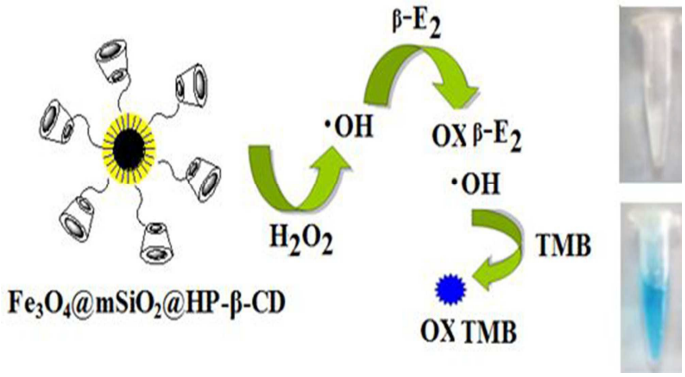

Schematic illustration of colourimetric detection of β-E_2 by using Fe_3O_4@mSiO_2@HP-β-CD nanoparticles catalyzed color reaction.